Hindawi
Advances in Civil Engineering
Volume 2021, Article ID 8886557, 13 pages
https://doi.org/10.1155/2021/8886557

Research Article

Dynamic Response Analyses of Plastic Greenhouse Structure considering Fluctuating Wind Load

Yingchun Jiang,[1] **Yikui Bai**,[2] **Cong Wang**,[2] **Yonggang Wang**,[3] **and Xinfu Pang**[4]

[1]*College of Engineering, Shenyang Agricultural University, Shenyang 110866, China*
[2]*College of Water Conservancy, Shenyang Agricultural University, Shenyang 110866, China*
[3]*College of Information and Electrical Engineering, Shenyang Agricultural University, Shenyang 110866, China*
[4]*School of Automation, Shenyang Institute of Engineering, Shenyang 110136, China*

Correspondence should be addressed to Yikui Bai; baiyikui@syau.edu.cn

Received 14 August 2020; Revised 15 December 2020; Accepted 30 December 2020; Published 15 January 2021

Academic Editor: Dan Ma

Wind load is one of the main factors of plastic greenhouse collapse. To solve the dynamic response problem of greenhouses under wind load and determine the dangerous section of a skeleton structure, the investigated lump method is presented for the dynamic response analysis of a plastic greenhouse, considering pulsating wind on the basis of Timoshenko beam theory. First, the investigated lump is designed according to the Timoshenko beam microbody concept. On the basis of Timoshenko beam theory, the governing equations of the skeleton structure of the greenhouse are derived, and the realization process of the algorithm is also provided. Second, the accuracy and effectiveness of the proposed numerical method are verified by an example in which the bending wave of a variable cross section beam with free ends propagates. Finally, the dynamic response of the steel skeletons of plastic greenhouses is analyzed under the effect of the simulation wind speed, and the spatial distribution of the maximum node displacement and the section maximum stress of the steel skeleton are obtained. Computational results show that the displacement peak is near the top of the plastic greenhouse. The most dangerous section of the top chord in the steel skeleton is near the leeward bottom, which has a maximum stress of 219.4 MPa, and the most dangerous section of the bottom chord is near the 1 m height on the leeward side of the plastic greenhouse, which has a maximum stress of 248.5 MPa. Bending stress is the main factor of the rapid increase of stress at the bottom of the skeleton. The maximum node displacement and cross-sectional stress caused by fluctuating wind loads are higher than those caused by average wind loads. The fluctuating wind load should be considered in the wind-induced response analyses of plastic greenhouses.

1. Introduction

1.1. Literature Review. Greenhouses are an important facility for modern agriculture and have made outstanding contributions to the development of modern agriculture. Greenhouses are also a special form of agricultural construction. In addition to providing animals and plants with the basic space for growth and production and an environment with suitable temperature and humidity, greenhouses must also bear many kinds of loads caused by abnormal operating conditions and extreme natural disasters (e.g., blizzard, gale, and hail). Abnormal weather conditions, such as strong winds and heavy snow, can deform plastic greenhouse structures severely and cause collapses [1, 2]. The safety of greenhouse structures and their bearing capacity has gradually warranted attention with the continuous development of greenhouses. The steel skeleton of greenhouses and plastic greenhouses is a light-weight structure, with features, such as light dead weight, large span, and thin and long rods, that make the greenhouse structure sensitive to wind load. The influence of wind load on the skeleton structure is an important consideration in greenhouse structure design [3]. Performing time-history analysis under fluctuating wind load can lead to the accurate grasp of the stress characteristics of greenhouse and plastic greenhouse structures and provide a scientific reference for the

structural analysis and wind resistance design of greenhouses and plastic greenhouses. Experimental and numerical simulation methods are used to study the wind load and bearing capacity of greenhouse structures.

The data obtained from the test is important for studying the bearing capacity of greenhouse structures [4] and the wind pressure coefficient [2, 5–7]. However, due to the high cost of testing and the long cycle, testing cannot be performed for each structure, and a structure with an optimized wind resistance performance is difficult to obtain. The numerical simulation of greenhouse structures has been developed rapidly with the development of computers and numerical calculation methods. The wind pressure coefficients and their distribution on the surfaces of a single-span plastic greenhouse and a solar greenhouse have been investigated [8]. The critical wind speeds at which damage occurs on the surfaces of single-span plastic and solar greenhouses have been determined. The wind direction, spacing, and span of a greenhouse can influence the wind pressure distribution on the surface of greenhouses [6, 9, 10]. Maximum positive or negative pressure may cause the collapse of the greenhouse frame. By simulating the wind speed of the airflow around and through a greenhouse structure, the influence of strong lateral wind on the leakage rate and internal pressure coefficient of the greenhouse can be studied [11, 12]. The mechanical properties of various greenhouse frame structures have been studied under the action of wind load, snow load, and different load combinations [13, 14]. In a study, the safety wind speeds for single-span greenhouses were calculated and compared with the actual wind speeds and snow depths over a period of 8 years in different regions to analyze the structural safety of single-span greenhouses [15]. The calculation method for the critical load of a circular arch with out-plane bifurcation buckling was proposed [16] for the theoretical analysis for the wind resistance design of arched greenhouses.

The stress of the greenhouse covering material and the failure behavior of the film can affect the stress performance of different greenhouse frame structures [17, 18]. Unfavorable load combination, such as wind and snow, is one of the reasons for the collapse of arched multispan greenhouse structures [19]. An obvious stress concentration exists at the connection between the truss arch and longitudinal beam of plastic greenhouses. The equivalent stress and displacement of some components exceed the allowable range, and the safety of greenhouse structures is mainly controlled by their strength and rigidity [20]. The maximum bending moment of single-span arched greenhouses appears at the bottom of the windward side wall [21]. The connection modelling condition of the skeleton structure of greenhouses and the addition of the support modelling condition can affect the vibration modes of multispan greenhouses [22]. The fatigue life of greenhouses can be predicted accurately by using a fatigue stress model, considering the dead weight and the wind speed [23]. Complex stress state caused by combination of dead load and wind load was modeled via CFD to examine its effect on the variation of stress distribution in the greenhouse structure [24]. An improved model was established to predict the permeability evolution by the fractal dimension, and strategies for overburden aquifer protection were proposed [25]. A damage-based model of coupled thermal-flowing-mechanical effects was adopted to illustrate the mechanical principle of gas fracturing and simulate the coupled process during the gas fracturing [26].

1.2. Motivation. When studying the bearing capacity and stress characteristics of a greenhouse structure, wind is usually applied to the greenhouse structure in the form of a quasistatic load. Wind speed can be composed of the mean and fluctuating winds. Instantaneous wind force is the most disadvantageous to light-weight greenhouse structures, and a few seconds of instantaneous wind can destroy an entire skeleton structure.

Using a 10 min time-distance is unsafe for greenhouse structures [27]. However, few studies on the pulsating wind effect on the mechanical properties of greenhouses have been conducted. The time-history analysis of greenhouse structures under wind loads can lead to an accurate grasp of the stress characteristics of the structures. For example, Hur and Kwon [23] did not perform time-history analysis on wind speed when they studied the safety of greenhouse structures under dynamic wind loads. Therefore, the effect of fluctuating wind load on the dynamic response of greenhouse structures should be studied further through time-history analysis.

In this study, from the perspective of the wave propagation of greenhouse structures and on the basis of Timoshenko beams theory, considering shear deformation and rotational inertia, a calculation method for the dynamic response time-history analysis of greenhouse structures under wind load is proposed, and the dynamic response of the steel skeleton structure of a greenhouse is analyzed. The time-history analysis of greenhouses can lead to the accurate grasp of the stress characteristics of skeleton structures under dynamic action, providing meaningful results for the dynamic analysis and wind-resistant design of greenhouse structures.

2. Principle of Calculation

According to the equilibrium conditions of a microunit, the dynamic equilibrium equation of the Timoshenko beam [28], considering shear deformation and rotational inertia, is obtained as follows:

$$\rho A \frac{\partial^2 u}{\partial t^2} = \frac{\partial V}{\partial x} + q(x), \tag{1}$$

$$\rho I \frac{\partial^2 \theta}{\partial t^2} = \frac{\partial M}{\partial x} + V, \tag{2}$$

where ρ is the material density, kg/m^3; A is the cross-sectional area, m^2; u is the transverse displacement of the neutral axis of the beam, m; t is the time, s; V is the shear force of any cross section, N; x is the any cross-sectional position, m; $q(x)$ is the transverse force per unit length on the beam, N/m; I is the second moment of the area, m^4; θ is

the section angle caused by bending deformation, rad; and M the bending moment of any cross section, N·m.

In Timoshenko's theory, the total rotation angle of the neutral axis of the beam can be composed of two parts: the section angle caused by bending deformation and the rotation angle of the neutral axis caused by shear deformation:

$$\frac{\partial u}{\partial x} = \theta + \gamma, \tag{3}$$

where $(\partial u/\partial x)$ is the total rotation angle of the beam's neutral axis, rad; and γ is the rotation angle of the neutral axis caused by shear deformation, rad.

The shear force and strain relationship is

$$V = kGA\gamma = kGA\left(\frac{\partial u}{\partial x} - \theta\right). \tag{4}$$

The bending moment and curvature relationship is

$$M = EI\frac{\partial \theta}{\partial x}, \tag{5}$$

where E is the elastic modulus, N/mm^2; G is the shear modulus, N/mm^2; and k is the section shear correction coefficient.

3. Dynamic Response Analysis Method for Steel Skeleton Structure of Greenhouse

The dynamic response of the steel skeleton structure is obtained to simulate the propagation process of the bending wave in the steel skeleton structure of a greenhouse. First, the composition of the investigated lump of the greenhouse skeleton structure is provided based on Timoshenko beam microunits. The dynamic equilibrium and rotation equations of the investigated lump are established based on the Timoshenko beam's dynamic equation. On the basis of the shear force and strain, bending moment and curvature, and axial force and strain relationships of beam theory, the relationship between the internal force and displacement in a discrete segment is obtained. Then, by applying the equations provided above and computing alternately in the time domain, the numerical method is presented for the dynamic response analyses of a greenhouse structure. Finally, the effectiveness of the investigated lump method is verified. The strategic structure of the dynamic response analysis method for greenhouse structures is shown in Figure 1.

3.1. Governing Equations of the Greenhouse Skeleton Structure

3.1.1. Mechanical Model of Skeleton Structure. The steel skeleton structure of the greenhouse is divided into discrete spaces by nodes (Figure 2). Discrete segment l exists between nodes i and j. The investigated lumps are composed of half of the spatial discrete segments associated with the nodes, and the endpoint number of discrete segments can be used to represent the number of investigated lumps. Investigated lump i is composed of half of the top chord and the web member connected to node i, that is, the area surrounded by the dotted ellipse on the left. Investigated lump k is composed of half of the bottom chord and the web member connected to node k, that is, the area surrounded by the dotted ellipse on the right.

Figure 3 shows the spatial position and central internal force diagram of discrete segment l of investigated lump i. Let n be the number of components associated with investigated lump i, and the force of the investigated lump comes from the wind pressure and the internal force of the central section of the discrete members of the structure. In Figure 3, x and z are the global coordinate axes, and x' and z' are the local coordinate system axes. φ_l is the angle between the x' axis of the local coordinate system and the x axis of the global coordinate system of discrete segment l, rad. N_l and V_l, respectively, represent the axial and shear forces acting on the central section of discrete segment l, N. M_l is the bending moment of the central section of discrete segment l, N·m, and N_i and V_i, respectively, represent the axial and shear forces of the i-end section of discrete section l, N. $M_i$is the bending moment of the i-end section of discrete section l, N·m. $N_j$and V_j, respectively, denote the axial and shear forces of the j-end section of discrete section l, N. $M_j$is the bending moment of the j-end section of discrete section l, N·m. L_l is the length of discrete segment l, m. $q(x')$is the external load of discrete segment l, N/m.

According to equation (1), the discrete form of the dynamic equilibrium equation for the translational motion of the investigated lump can be established using Figure 3. That is,

$$m_i\ddot{u}_i = \sum_{l=1}^{n}\left(N_l\cos\varphi_l - V_l\sin\varphi_l\right) + \sum_{l=1}^{n}F_{ql}\cdot\sin\varphi_l, \tag{6}$$

$$m_i\ddot{w}_i = \sum_{l=1}^{n}\left(N_l\sin\varphi_l + V_l\cos\varphi_l\right) - \sum_{l=1}^{n}F_{ql}\cdot\cos\varphi_l, \tag{7}$$

where $m_i = \sum_{l=1}^{n}(m_l/2)$ is the mass of investigated lump i, and m_l is the mass of discrete section l, kg.

$\ddot{u}_i$ and $\ddot{w}_i$ are the accelerations of investigated lump i along the x-axis and z-axis directions, respectively, m/s^2. F_{ql} is the resultant force of transverse distributed load $q(x')$ on discrete segment l, that is, $F_{ql} = \int_0^{L_l/2} q(x')\mathrm{d}x'$.

According to equation (1), the discrete form of the dynamic equilibrium equation for the rotational motion of the investigated lump can be established using Figure 3. That is,

$$J_i\ddot{\theta}_i = \sum_{l=1}^{n}\left(M_l - V_l\frac{L_l}{2}\right) + \sum_{l=1}^{n}M_{ql}, \tag{8}$$

where $J_i = \sum_{l=1}^{n}(1/3)\cdot(m_l/2)\cdot(L_l/2)^2$ is the moment of inertia of investigated lump i, kg·m^2. $\ddot{\theta}_i$ is the angular acceleration of investigated lump i around the endpoint axis, rad/s^2. M_l is the bending moment of the central section of

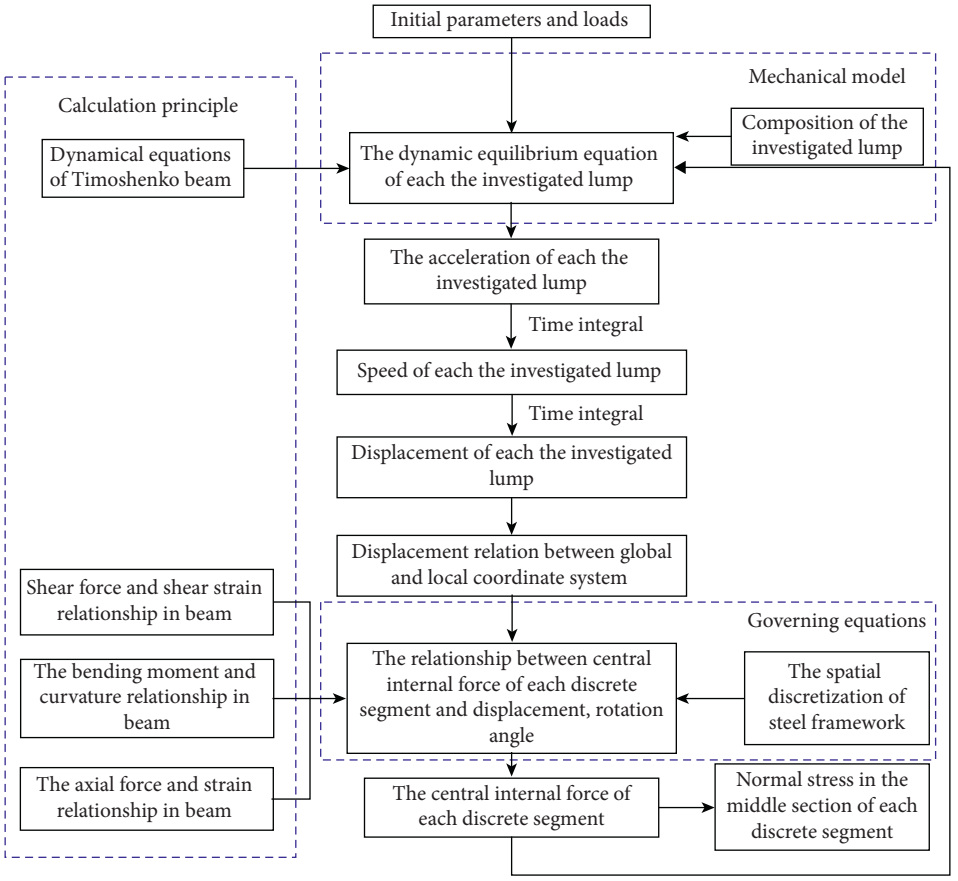

Figure 1: Method structure of dynamic response analysis for greenhouse.

discrete segment l, N·m. M_{ql} is the moment of distributed load $q(x')$ on discrete segment l to point i; that is, $M_{ql} = \int_0^{L_l/2} q(x')x'\,\mathrm{d}x'$.

3.1.2. Relationship between Internal Force and Displacement in Discrete Segments of Skeleton Structure. By the spatial discretization of equations (4) and (5), the shear force (V_l) and bending moment (M_l) of the central section of discrete segment l are obtained as follows:

$$V_l = k_l G_l A_l \left(\frac{w_j' - w_i'}{L_l} - \frac{\theta_i' + \theta_j'}{2} \right) = \frac{k_l G_l A_l}{L_l} \left[\left(w_j' - w_i' \right) - \frac{\theta_i' + \theta_j'}{2} L_l \right], \tag{9}$$

$$M_l = E_l I_l \frac{\left(\theta_j' - \theta_i' \right)}{L_l}, \tag{10}$$

where E_l is the elastic modulus of discrete segment l, N/mm^2. I_l is the second moment of the area, m^4. G_l is the shear modulus, N/mm^2. A_l is the cross-sectional area of discrete segment l, m^2. k_l is the section shear correction coefficient of discrete segment l.$w_i'$and w_j' are the respective transverse displacements of the i- and j-ends of discrete section l, m. θ_i'

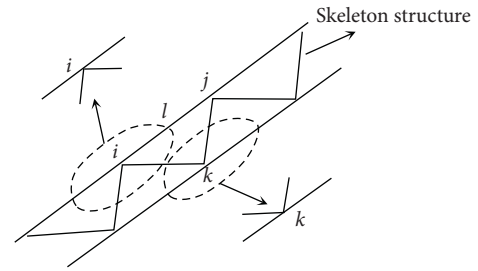

Figure 2: Investigated lumps of skeleton structure.

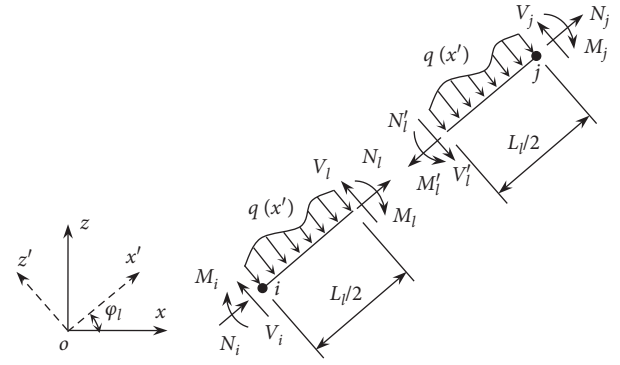

Figure 3: Free-body diagram of discrete section l of investigated lumps.

and θ_j' are the respective rotation angles of the i- and j-ends of discrete section l, m.

According to the relationship between the axial force and strain of beam theory, the axial force of the central section of discrete segment l can be obtained as follows:

$$N_l = \frac{E_l A_l}{L_l}\left(u_j' - u_i'\right), \tag{11}$$

where u_i' and u_j' are the respective axial displacements of the i- and j-ends of discrete section l, m.

The total normal stress of the cross section is the sum of the bending and axial normal stresses. From formulas (10) and (11), the total normal stress of the cross section can be obtained as

$$\sigma = \frac{|M_l|}{W_y} + \frac{|N_l|}{A_l}, \tag{12}$$

where W_y is the section modulus in bending, mm^3.

3.1.3. Displacement Relation between Local and Global Coordinate System. The dynamic equilibrium equation of investigated lump i is established in the global coordinates, and the constitutive equation of internal force at the central section is established in the local coordinate system. Therefore, the displacement relationship between the local and global coordinate systems must be established.

The transformation equation from the global to the local coordinate system is

$$\begin{cases} u_i' = u_i \cos\varphi_l + w_i \sin\varphi_l, \\ w_i' = -u_i \sin\varphi_l + w_i \cos\varphi_l, \\ \theta_i' = \theta_i. \end{cases} \tag{13}$$

The transformation equation from the local to the global coordinate system is

$$\begin{cases} u_i = u_i' \cos\varphi_l - w_i' \sin\varphi_l, \\ w_i = u_i' \sin\varphi_l + w_i' \cos\varphi_l, \\ \theta_i = \theta_i'. \end{cases} \tag{14}$$

3.2. Algorithm Implementation. Wind force is derived from the wind speed calculation, and the time-history of wind force is applied to the skeleton structure. The dynamic equilibrium equation of the investigated lump and the relationship between the central section internal force and the displacement in the discrete segment of the skeleton structure are alternately used, and the displacement relationships between the local and global coordinate systems are combined. Computing alternately in the time domain realizes the dynamic response analysis of the greenhouse steel skeleton structure. The pseudocode of this method is presented in Algorithm 1.

3.3. Method Validation. The flexural wave propagation of a variable cross section beam with two free ends is calculated by using the investigated lump method. The calculation results are compared with those of the finite difference method in reference [29] to verify the correctness and effectiveness of the proposed numerical algorithm method.

The elastic modulus (E) of the beam is 209 GPa, the density (ρ) is 8000 kg/m^3, Poisson's ratio (ν) is 0.3, the shear modulus (G) is 80.4 GPa, and the shear cross section correction coefficient (k') is 0.886. The length of the beam (X) is 5 m. The beam section changes at the middle point, the radius of the left half is 0.1 m, and the radius of the right half is 0.08 m. The number of discrete segments is 200 in the length direction for the uniform beam, and the calculation time step of this paper is $\Delta t = 1.25\,\mu s$. The length from the left end of the beam is x, and the bending moment at the section is M.

After normalization, time $\overline{t}$ is $(1/X)\sqrt{(E/\rho)}t$, the length from the left end of the beam is $\overline{x} = (x/X)$, the lateral displacement is $\overline{w} = (w/X)$, and the bending moment is $\overline{M} = (MX/EI)$.

The inclination moment of the left end of the beam is

$$\overline{M}_1 = \begin{cases} \dfrac{\overline{t}}{\overline{t}_0}, 0 \le \overline{t} \le \overline{t}_0, 1, \overline{t} > \overline{t}_0. \end{cases} \tag{15}$$

Figure 4 shows the time-history comparison curve at a position with a length of $\overline{x} = 0.2$ from the left end of the beam. Figure 4(a) presents the time-history comparison curve of transverse displacement $\overline{w}$, and Figure 4(b) presents the time-history comparison curve of bending moment $\overline{M}$. The calculation results of the proposed numerical algorithm are nearly the same as those of the finite difference method. The comparison results show that the presented algorithm has good numerical calculation accuracy and is suitable for the dynamic response of the greenhouse steel skeleton.

4. Analysis of Dynamic Response of Plastic Greenhouse Steel Skeleton Structure

4.1. Calculation Model and Parameters of Plastic Greenhouse Steel Skeleton. The research object is a plastic greenhouse steel skeleton structure, which adopts a single flat plane frame model (Figure 5). The diameter of the steel pipe of the top chord is 33 mm, and the wall thickness of the steel pipe is 3.3 mm. The diameter of the bottom chord reinforcement is 12 mm, and that of the web member is 8 mm. The strength grade of the reinforcement is HPB 300. The skeleton structure has 55 nodes, that is, 55 investigated lumps. The nodes are numbered from left to right, with those at the top chord set to 1–28, as shown in nodes 5, 15, and 24. The example is represented as a solid point. The nodes at the bottom chord are numbered 29–55, as shown in nodes 33, 42, and 52. Each segment between nodes is regarded as a discrete segment, with a total of 107 discrete segments. The discrete segments are numbered from left to right, with the segments at the top chord set to ①–㉗, and those at the bottom chord to ㉘–㊸. The web members are numbered ㊹–㉗. The calculation time step is 0.05 ms.

Input: Time Step Δt, Total time steps T; Total number of discrete segments n, Discrete length L_l, $l \in n$; Total number of investigated lump R, Mass of investigated lump m_i, Moment of inertia of investigated lump J_i, $i \in R$; Load point R_f, $R_f \in R$; fluctuating wind speed v_i,$i \in R_f$; Constraint point R_c.
Output: The displacement of investigated lumps u_i and w_i, rotation angle θ_i, maximum stress $\sigma_{\max}$, shear forces at ends of discrete segment V_i and V_j, bending moments at ends of discrete segment M_i and M_j.
Initialization: $u_i = 0$, $w_i = 0$, $\theta_i = 0$, $i \in R$; $N_l = 0$, $V_l = 0$, $M_l = 0$, $l \in n$.

(1) **do** $j = 1, T$
(2) **do** $l = 1, n$
(3) Calculate external load F_{ql}.
(4) **end do**
(5) **end do**
(6) **do** $j = 1, T$
(7) **do** $l = 1, n$
(8) External force in the x direction at loading point $\sum_{l=1}^{n} F_{ql} \cdot \sin\varphi_l$ in equation (6), external force in the y direction $-\sum_{l=1}^{n} F_{ql} \cdot \cos\varphi_l$ in equation (7), Moment $\sum_{l=1}^{n} M_{ql}$ in equation (8).
(9) **end do**
(10) Define constraints: $u_i = 0$, $w_i = 0$, $\theta_i = 0$,$i \in R_c$.
(11) **do** $l = 1, n$
(12) Calculate u_i', u_j' and w_i', w_j' at both ends of segment l by equation (13). Calculate N_l by equation (11), Calculate V_l by equation (9), Calculate M_l by equation (10), Calculate $\sigma_{\max}$ by equation (12); Calculate V_i and V_j by equation (11),
(13) **end do**
(14) **do** $l = 1, n$
(15) Calculate u_i, u_j and w_i, w_j at both ends of segment l by equation (14), Calculate the force and moment of the investigated lump $\sum_{l=1}^{n} (N_l \cos\varphi_l - V_l \sin\varphi_l)$ in equation (6) $\sum_{l=1}^{n} (N_l \sin\varphi_l + V_l \cos\varphi_l)$ in equation (7), $\sum_{l=1}^{n} (M_l - V_l (L_l/2))$ in equation (8)
(16) **end do**
(17) **do** $i = 1, R$
(18) Calculate acceleration of the investigated lump $\ddot{u}_i$ in equation (6),$\ddot{w}_i$ in equation (7) and angular acceleration$\ddot{\theta}_i$ in equation (8).
(19) **if** $i \in R_f$ **then**
(20) superimposing Step 8, Calculate acceleration of the investigated lump $\ddot{u}_i$ in equation (6),$\ddot{w}_i$ in equation (7), angular acceleration $\ddot{\theta}_i$ in equation (8).
(21) **end if**
(22) Calculate velocity $\dot{u}_i = \dot{u}_i + \ddot{u}_i \Delta t$, $\dot{w}_i = \dot{w}_i + \ddot{w}_i \Delta t$ and angular velocity $\dot{\theta}_i = \dot{\theta}_i + \ddot{\theta}_i \Delta t$
(23) **end do**
(24) **do** $i = 1, R$
Calculate displacement $u_i = u_i + \dot{u}_i \Delta t$, $w_i = w_i + \dot{w}_i \Delta t$ and rotation angle $\theta_i = \theta_i + \dot{\theta}_i \Delta t$
(25) **end do**
(26) **end do**

Algorithm 1: The numerical method of dynamic response analysis for greenhouse structure.

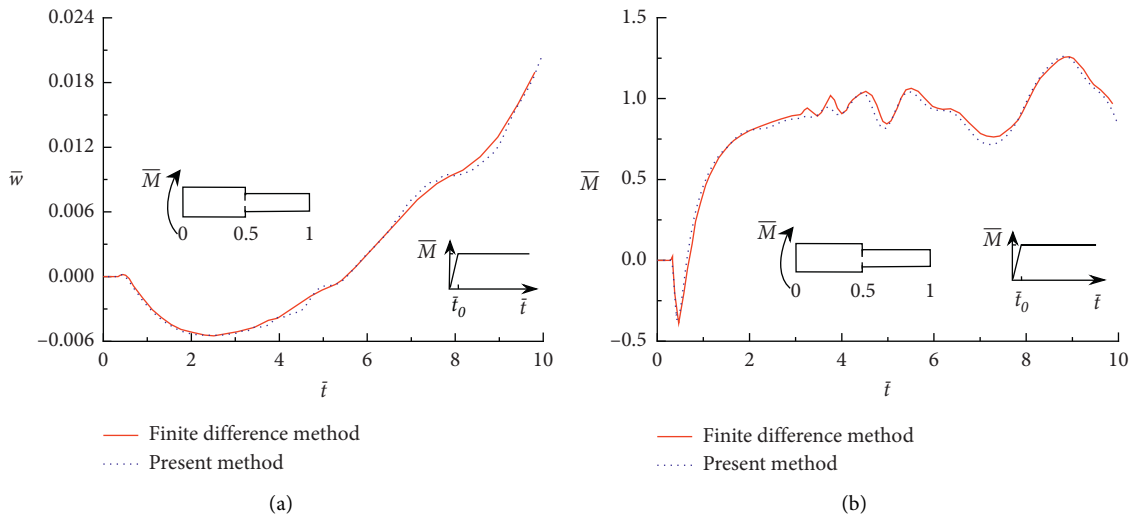

Figure 4: Time-history contrast curve at the $\bar{x} = 0.2$ from the left end of the beam. (a) Time-history contrast curve of the transverse displacement $\bar{w}$. (b) Time-history contrast curve of the bending moment.$\bar{M}$

4.2. Wind Load Time-History Simulation. The wind load must be used as the input load parameter for the dynamic response analysis of the plastic greenhouse steel frame of the plane frame model. In this study, the input load parameters needed for calculation are obtained through the numerical simulation of wind speed.

According to reference [30], the input wind load parameters are obtained by calculation. The average wind speed at 10 m above the ground is 29.67 m/s. According to reference [3], the terrain roughness index of the plastic greenhouse structure is 0.16, and the terrain roughness coefficient is 0.03.

Using the Davenport spectrum and harmonic superposition method [31], the fluctuating wind speed of each space point on the surface of the plastic greenhouse shown in Figure 5 is simulated.

The fluctuating wind is assumed to be a stationary Gaussian random process with a zero mean. Fluctuating wind speed $v_j(t)$ can be expressed as follows:

$$v_j(t) = \sum_{k=1}^{j} \sum_{l=1}^{S} \left|H_{jk}(f_l)\right| \sqrt{2 \cdot 2\pi\Delta f} \cos\left[2\pi f_l t + \alpha_{jk}(f_l) + \beta_{kl}\right], \tag{16}$$

where S is the sampling points of the fluctuating wind frequency, and j is the number of simulation points. $H_{jk}(f_l)$ represents the elements in the lower triangular matrix. $\Delta f = ((f_u - f_d)/S)$ is the frequency increment, and f_u and f_d are the upper and lower limits of the fluctuating wind interception frequency, respectively. β_{kl} represents random numbers that are uniformly distributed between 0 and 2π.

The wind pressure ($W(z,t)$) at height z in the downwind direction can be obtained through the wind speed:

$$W(z,t) = \frac{1}{2}\rho v'^2(x,y,z,t) = \frac{1}{2}\rho[\overline{v}(z) + v(x,y,z,t)]^2 = \frac{1}{2}\rho\overline{v}(z)^2 + \frac{1}{2}\rho\left[2\overline{v}(z)v(x,y,z,t) + v(x,y,z,t)^2\right], \tag{17}$$

where ρ is the air density, $\overline{v}(z)$is the mean wind speed at height z, $v(x,y,z,t)$ is the fluctuating wind speed at height z, $(1/2)\rho\overline{v}(z)^2$ is the mean wind pressure at height z, and $(1/2)\rho[2\overline{v}(z)v(x,y,z,t) + v(x,y,z,t)^2]$ is the fluctuating wind pressure at height z.

Figure 6 shows the time-history curve of the fluctuating wind speed at nodes 4 and 10. Figure 7 compares the simulated wind speed power spectrum of nodes 4 and 10 with the Davenport fluctuating wind speed power spectrum. The figure indicates that the change trend of the simulated power spectrum is consistent with the target power spectrum. Figure 8 shows the spatial coherence comparison at different points. The figure shows that the wind speed at two adjacent points (e.g., points 3 and 4) has the strongest coherence. The maximum value of the normalized cross-correlation function ($R_{\max}$) is 0.9681, and that of points 3 and 10 is $R_{\max} = 0.8669$. The coherence of wind speeds at two adjacent points is strong. The coherence of wind speed gradually weakens with the increase of the distance between the two points, which conforms to the coherence law of the wind field.

The fluctuating wind speed's time-history at different points of the plastic greenhouse can be verified by Figures 7 and 8.

Figure 9 shows the time-history curve of the fluctuating wind pressure at points 4 and 10 on the surface of the plastic greenhouse structure obtained by simulation. The input wind pressure time-history of the plastic greenhouse skeleton structure can be obtained by the superposition of the fluctuating and mean wind pressures' time-history [30]. The left side of the plastic greenhouse is the windward side, as shown in Figure 5.

4.3. Analysis of Calculation Results

4.3.1. Spatial Distribution of Maximum Displacement of Node. Figure 10 shows the spatial distribution curve of the maximum displacement of each node of the plastic greenhouse skeleton structure with a span of 10 m. "Mean + Fluctuating" in the figure represents the calculated results considering both the mean and fluctuating wind loads. "Fluctuating" represents the calculated results considering only the effect of the fluctuating wind load. "Mean" represents the calculated results considering only the effect of the mean wind load.

Figure 10 shows that the displacement of the top chord increases significantly between nodes 10 and 19, the maximum displacement at node 15 is 20.5 mm, and secondary peaks of displacement appear at nodes 5 and 24. The displacement of the bottom chord increases significantly between nodes 38 and 46. The maximum displacement at node 42 is 20.8 mm, and secondary peaks appear at nodes 33 and 52. Figure 5 shows that the displacement value of the top chord of plastic greenhouses above the 2.5 m height increases significantly, the displacement peak appears at the top of the plastic greenhouse, and the second peak is at the 1.5 m height on the windward and leeward sides. The

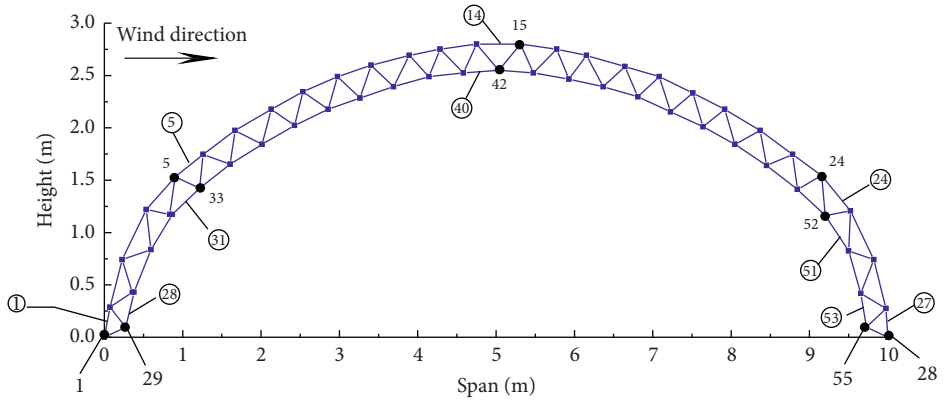

Figure 5: Steel skeleton structure of the plastic greenhouse.

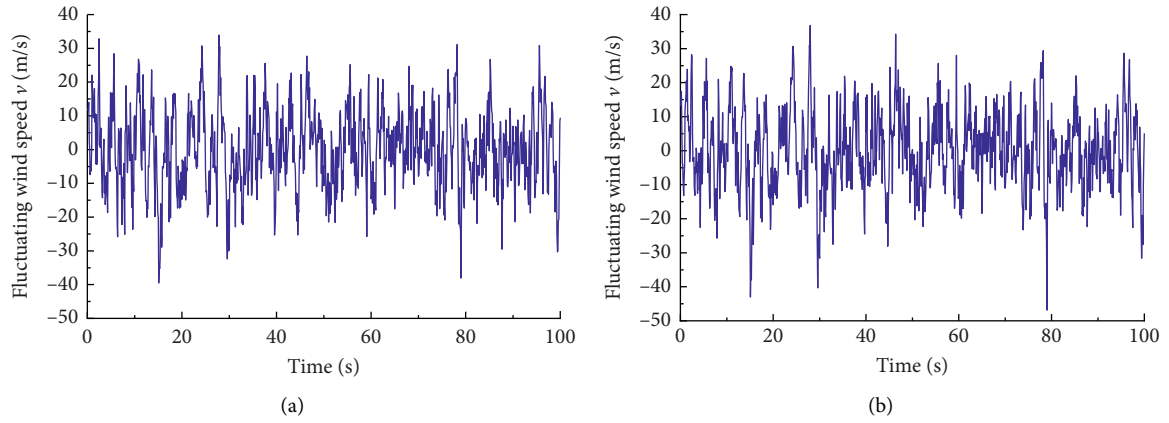

Figure 6: Time-history curve of fluctuating wind speed of plastic greenhouse. (a) Node 4. (b) Node 10.

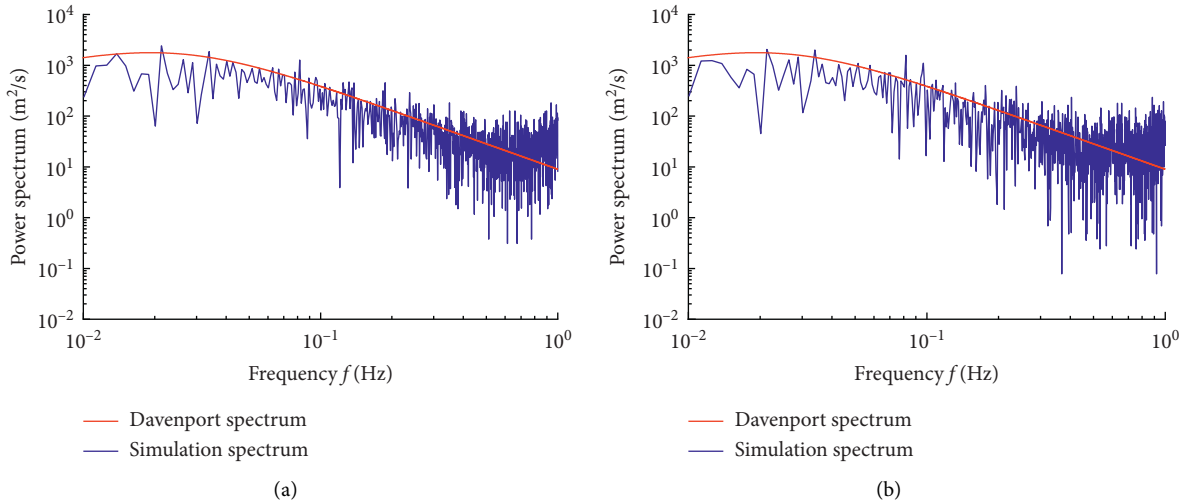

Figure 7: Fluctuating wind power calculation power spectrum contrasting with target power spectrum. (a) Node 4. (b) Node 10.

displacement value of the bottom chord of plastic greenhouses above the 2.25 m height increases significantly, and the second peak is at the 1.4 m height on the windward sides and at the 1.2-m height on the leeward sides.

Figure 11 shows the structural displacement deformation diagram when the maximum displacement occurs at 27.9 s, considering both the mean and fluctuating winds. The displacement in the figure is magnified 20 times, and the

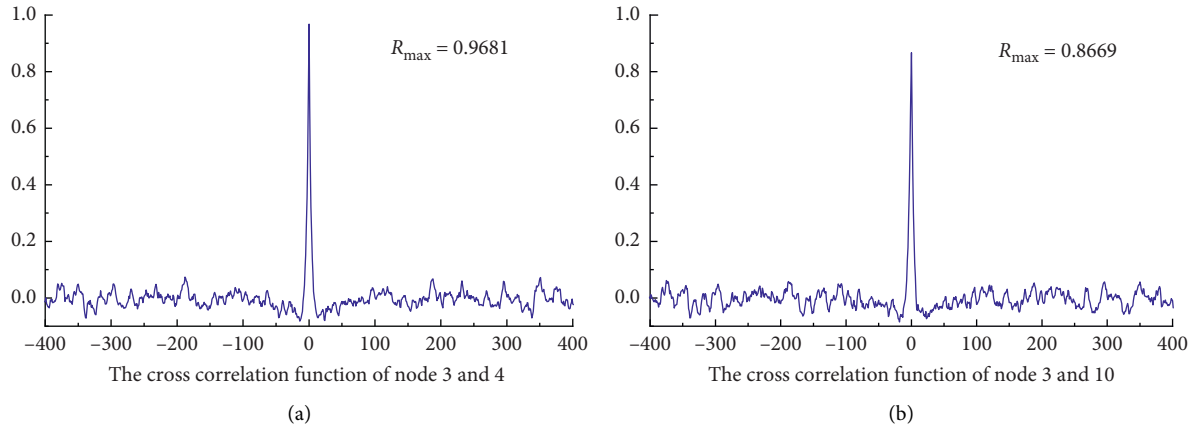

FIGURE 8: Normalized cross-correlation function of different nodes. (a) Cross-correlation function of points 3 and 4. (b) Cross-correlation function of points 3 and 10.

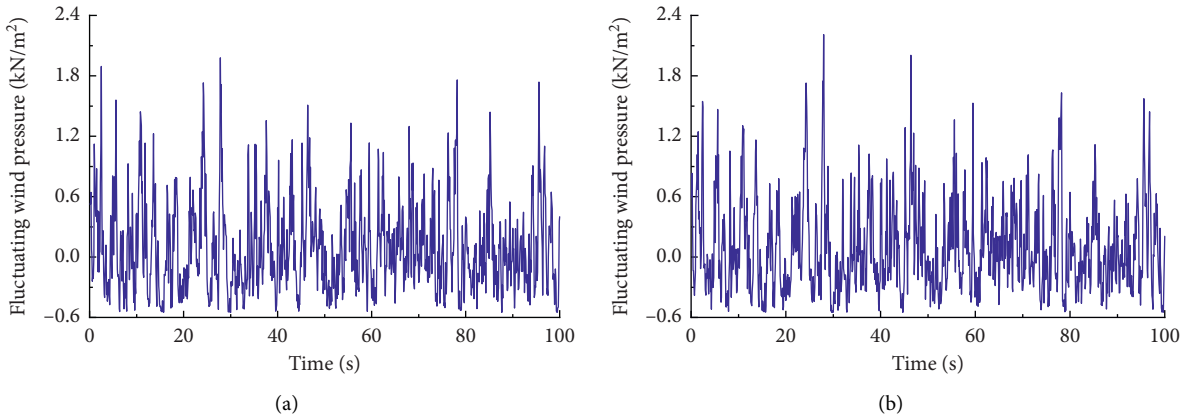

FIGURE 9: Fluctuating wind pressure time-history curve in different space nodes. (a) Node 4. (b) Node 10.

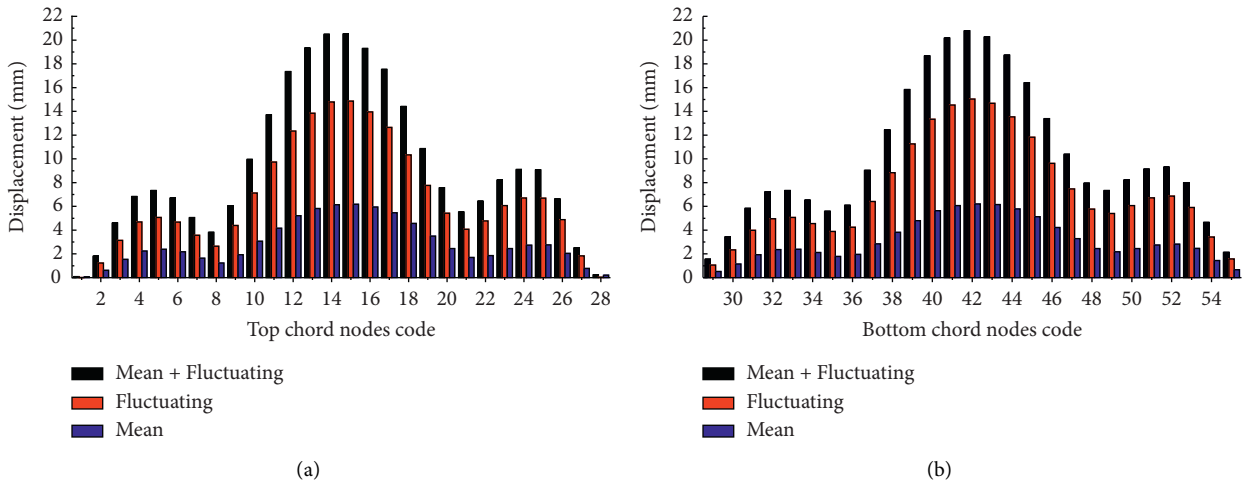

FIGURE 10: Distribution curves of the maximum displacement at nodes of plastic greenhouse. (a) Top chord. (b) Bottom chord.

position of the maximum displacement can be seen directly in the figure.

Table 1 shows the relative peak value of node displacement in the node displacement curve. The ratio multiples under different load conditions show that the maximum value of nodal displacement considering both the mean and fluctuating winds is approximately 1.4 times that considering only the fluctuating wind load, and 3.0–3.4

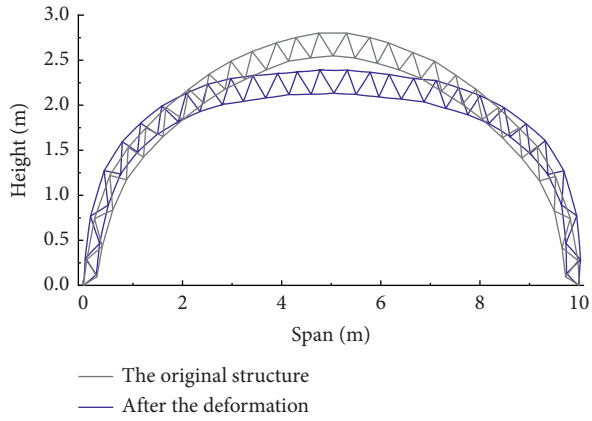

Figure 11: Structural displacement deformation diagram of plastic greenhouse at 27.9s when considering both the mean wind and the fluctuating wind.

Table 1: Comparison of nodal displacement (unit: mm).

Load		Cross section					
		Top chord			Bottom chord		
		5	15	24	33	42	52
Load	Mean + Fluctuating	7.3	20.5	9.1	7.3	20.8	9.3
	Fluctuating	5.1	14.9	6.7	5.1	15.0	6.9
	Mean	2.4	6.2	2.7	2.4	6.2	2.8
Ratio	(Mean + Fluctuating)/Fluctuating	1.4	1.4	1.4	1.4	1.4	1.4
	(Mean + Fluctuating)/Mean	3.0	3.3	3.4	3.0	3.4	3.3
	Fluctuating/Mean	2.1	2.4	2.5	2.1	2.4	2.5

times that considering only the mean wind load. The fluctuating wind load alone is 2.1–2.5 times that of the mean wind load alone.

The comparison results in Figure 10 and Table 1 indicate that the maximum displacement of each node is the largest under "Mean + Fluctuating," followed by that under "Fluctuating," and that under "Mean" is the smallest. The effect of fluctuating wind on node displacement is significant.

4.3.2. Spatial Distribution of Maximum Total Stress in Cross-Section. Figure 12 shows the spatial distribution comparison curve of the maximum value of the total normal stress in the cross section of each discrete segment of the plastic greenhouse skeleton structure. Total normal stress is the sum of the absolute values of the axial and bending normal stresses. The "Mean + Fluctuating," "Fluctuating," and "Mean" in the figure are the same as those in Figure 10.

Figure 12 indicates that, for both the top and bottom chords, the maximum stress is generally the largest under "Mean + Fluctuating," followed by that under "Fluctuating," and that under "Mean" is the smallest, and the variation trend of the stress at each discrete section is basically the same under the three loads. For the top chord, the stress at the bottom of the greenhouse skeleton structure increased significantly, and the stress at the bottom of the leeward side reached the maximum space of 219.4 MPa. At the top position of the plastic greenhouse, at the 1.6 m height on the windward side, and at the 1.4 m height on the leeward side of the plastic greenhouse, the stress of the cross-section displays secondary peaks. The peak stress of the bottom chord is 248.5 MPa, which appears in section 51, that is, near the 1 m height of the leeward side; the stress value near at the 1.0–1.75 m height of the windward side and at the 0.6–1.75 m height of the leeward side is greater than that of the section near the top of the greenhouse skeleton.

The stress value of the web members below the 1 m height on the leeward side is larger, and the stress value of the adjacent web members changes greatly. The stress value of the web member near the bottom end of the windward side is smaller than that of the web member near the bottom end of the leeward side. The stress value of the web member near the top of the greenhouse skeleton is smaller near the location where the stress values of the top and bottom chords are the smallest, and the stress values of the web member increase instead, that is, near the 2.3 m height.

The above analysis indicates that both the top and bottom chords of the greenhouse skeleton have relative peaks near the top, namely, the 1.3–1.6 m height at the windward side and at the 1.3–1.4 m height at the leeward side. The most dangerous section of the top chord in the steel skeleton is near the leeward bottom, and the most dangerous section of the bottom chord is near the 1 m height on the leeward side of the plastic greenhouse. The section stress of the web members below the 1 m height is larger.

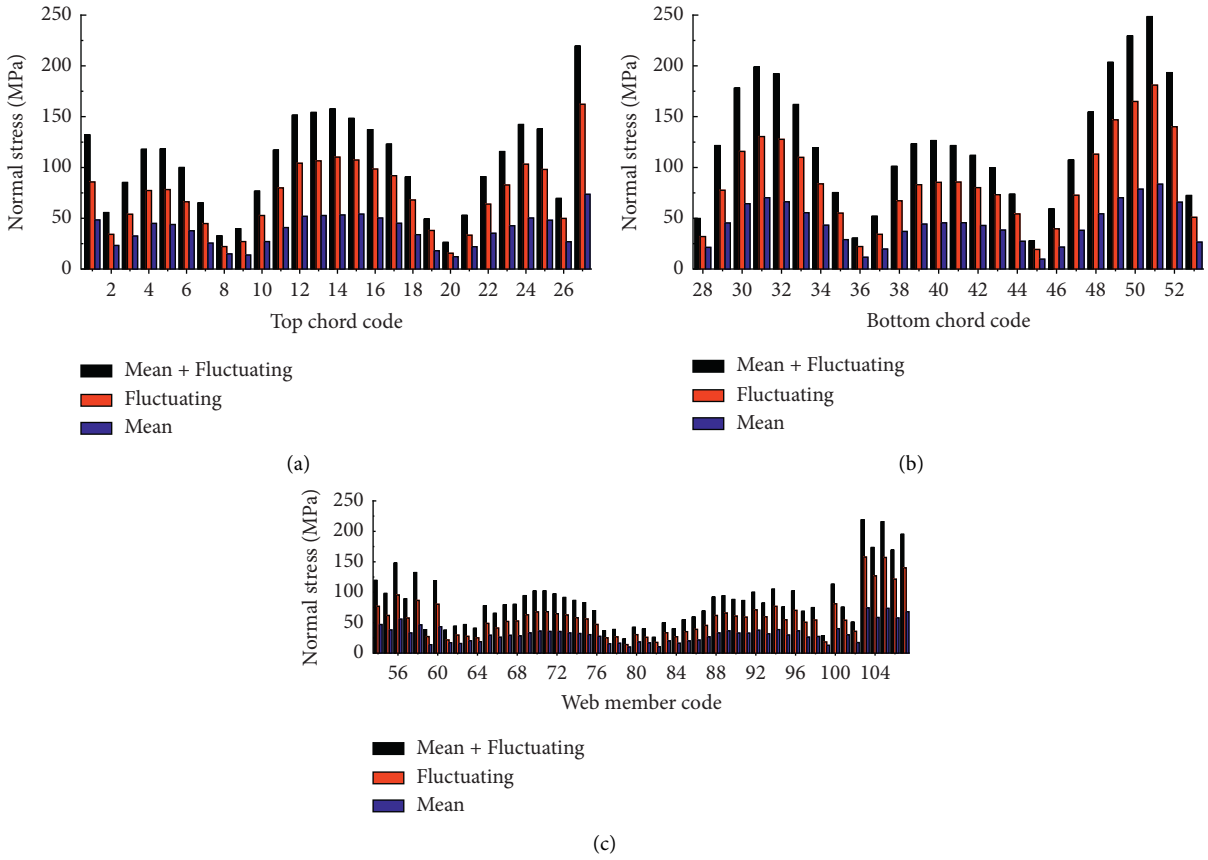

Figure 12: Distribution curve of maximum total stress at cross sections of plastic greenhouse. (a) Top chord. (b) Bottom chord. (c) Web member.

Table 2: Comparison of total stress at cross sections.

Load	Cross sections									
	Total stress at cross sections for top chord (MPa)					Total stress at cross sections for bottom chord (MPa)				
	1	5	14	24	27	28	31	40	51	53
Mean + Fluctuating	132.1	118.3	157.5	142.3	219.4	49.7	198.8	126.4	248.5	72.4
Fluctuating	85.8	78.2	110.2	103.3	162.1	31.9	130.4	85.3	181.1	51.0
Mean	48.3	43.8	54.1	50.3	73.5	21.3	70.2	45.5	83.6	26.5

Table 2 shows the relative peak stress of the top and bottom chords under different wind loads. The results in Figure 12 and Table 2 indicate that the effect of fluctuating wind on stress is basically consistent with the displacement.

4.3.3. Influence Law of Different Stress Components. Figure 13 shows the comparison curve of the stress components of each discrete section of the top chord under the action of both mean and fluctuating winds. The main component of the total stress is axial stress, but bending stress is the main component at sections 1, 2, 26, and 27 of the discrete section, that is, near the two bottom ends of the skeleton structure. For the plastic greenhouse structure, axial force is the main internal force, and the influence of bending moment on the internal force of both ends of the skeleton structure cannot be ignored.

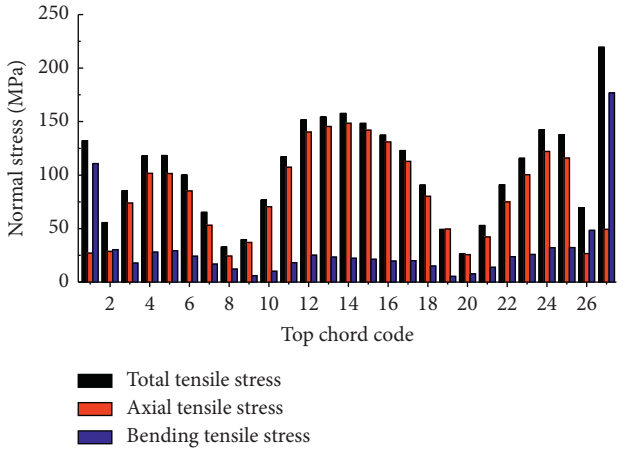

Figure 13: Comparison curve of stress component of discrete segments.

5. Conclusion

In this paper, the investigated lump method for the dynamic response analysis of plastic greenhouse structures under the wind load is presented. The accuracy and effectiveness of the proposed numerical method are verified by an example in which the bending wave of a variable cross section beam with free ends propagates. The physical meaning of the investigated lump is clear, and the classical dynamics equations are unnecessary.

Three conditions of numerical wind speed simulation (mean and fluctuating winds, fluctuating wind, and mean wind) are used as input load parameters for the dynamic response time-history analysis of a plastic greenhouse steel skeleton structure. The spatial distribution of the maximum value of node displacement and section stress in the dynamic response time-history record of the plastic greenhouse steel skeleton structure is obtained. The displacement of each node and the stress of each section are generally the largest under "Mean + Fluctuating," followed by those under "Fluctuating," and those under "Mean" are the smallest. The maximum values of node displacement and section stress under fluctuating wind load are approximately 2.5 and 2 times those of the mean wind load, indicating that the effect of fluctuating wind on the dynamic response of a plastic greenhouse steel skeleton structure is more important than that of mean wind. The relative peak values of node displacement appear near the top of the skeleton, at the 1.5 m height on the windward side, and at the 1.4 m and at the 1.2 m height on the leeward side. The relative peak values of cross section stress appear near the top of the skeleton, at the 1.3–1.6 m height on the windward side, and at the 1.3–1.4 m height on the leeward side. The most dangerous section of the top chord in the steel skeleton is near the leeward bottom, and the most dangerous section of the bottom chord is near the 1 m height on the leeward side of the plastic greenhouse. Axial stress is the main internal force of the greenhouse steel skeleton structure, and the section near the left end of the structure is the most dangerous. Bending stress is the main reason for the rapid increase of the stress at this location.

Data Availability

The analysis result data used to support the findings of this study are included within the article. The calculation data used to support the findings of this study are available from the corresponding author upon request.

Conflicts of Interest

The authors declare no conflicts of interest.

Acknowledgments

This study was supported in part by the National Natural Science Foundation of China (61673281, 61773269), Liaoning Provincial Key Research and Development Program (2018103007), Post Expert Project of National Bulk Vegetable Industry Technology System (CARS-23-C01), the Natural Science Foundation of Liaoning Province of China (2019-KF-03-01, 2019-KF-03-08), and the Program for Liaoning Excellent Talents in University (LR2019045).

References

[1] H. Moriyama, S. Sase, H. Kowata et al., "Engineering analysis of the greenhouse structures damaged by typhoon 0221 in Chiba and Ibaraki," *Journal of the Society of Agricultural Structures*, vol. 34, no. 3, pp. 199–212, 2003.

[2] H. Moriyama, S. Sase, L. Okushima, and M. Ishii, "Which design constraints apply to a pipe-framed greenhouse?" *Japan Agricultural Research Quarterly: JARQ*, vol. 49, no. 1, pp. 1–9, 2015.

[3] GB/T-51183-2016, *Code for the Design Load of Horticultural Greenhouse Structures*, China Planning Press, Beijing, China, 2016.

[4] G. Morcous, "Performance of conservatories under wind and snow loads," *Journal of Architectural Engineering*, vol. 15, no. 3, pp. 102–109, 2009.

[5] H. Moriyama, S. Sase, Y. Uematsu et al., "Wind tunnel study of the interaction of two or three side-by-side pipe-framed greenhouses on wind pressure coefficients," *American Society of Agricultural and Biological Engineers*, vol. 53, no. 2, pp. 585–592, 2010.

[6] H. Moriyama, S. Sase, Y. Uematsu et al., "Influence of ridge height of pipe-framed greenhouses on wind pressure coefficients," *American Society of Agricultural and Biological Engineers*, vol. 58, no. 3, pp. 763–769, 2015.

[7] K.-S. Kwon, D.-W. Kim, R.-W. Kim, T. Ha, and I.-B. Lee, "Evaluation of wind pressure coefficients of single-span greenhouses built on reclaimed coastal land using a large-sized wind tunnel," *Biosystems Engineering*, vol. 141, pp. 58–81, 2016.

[8] Z. Q. Yang, Y. X. Li, X. P. Xue, C. R. Huang, and B. Zhang, "Wind loads on single-span plastic greenhouses and solar greenhouses," *Horttechnology*, vol. 23, no. 5, pp. 622–628, 2013.

[9] R.-W. Kim, I.-B. Lee, and K.-S. Kwon, "Evaluation of wind pressure acting on multi-span greenhouses using CFD technique, Part 1: development of the CFD model," *Biosystems Engineering*, vol. 164, pp. 235–256, 2017.

[10] R.-W. Kim, S.-W. Hong, I.-B. Lee, and K.-S. Kwon, "Evaluation of wind pressure acting on multi-span greenhouses using CFD technique, Part 2: application of the CFD model," *Biosystems Engineering*, vol. 164, pp. 257–280, 2017.

[11] A. Mistriotis and S. Castellano, "Airflow through net covered tunnel structures at high wind speeds," *Biosystems Engineering*, vol. 113, no. 3, pp. 308–317, 2012.

[12] T. Kuroyanagi, "Investigating air leakage and wind pressure coefficients of single-span plastic greenhouses using computational fluid dynamics," *Biosystems Engineering*, vol. 163, pp. 15–27, 2017.

[13] J. G. V. Neto and J. Soriano, "Distribution of stress in greenhouses frames estimated by aerodynamic coefficients of Brazilian and European standards," *Scientia Agricola*, vol. 73, no. 2, pp. 97–102, 2016.

[14] C. Maraveas and K. D. Tsavdaridis, "Strengthening techniques for greenhouses," *AgriEngineering*, vol. 2, no. 1, pp. 37–54, 2020.

[15] J.-W. Lee, "Analysis of safety wind speed and snow depth for single-span plastic greenhouse according to growing crops,"

Current Research on Agriculture and Life Sciences, vol. 31, no. 4, pp. 280–285, 2013.

[16] J. J. Wang, M. Ding, X. G. Jiang et al., "Static analysis of circular curved beam with free torsion considering second-order moment effect," *Journal of China Agricultural University*, vol. 24, no. 3, pp. 109–116, 2019.

[17] M. Ding, M. M. Li, X. D. Shi et al., "Stable bearing capacity coculation of greenhouse structures considering skin effect of covering material," *Transactions of the Chinese Society of Agricultural Engineering*, vol. 32, no. S1, pp. 224–232, 2016.

[18] G. Dougka and D. Briassoulis, "Load carrying capacity of greenhouse covering films under wind action: optimising the supporting systems of greenhouse films," *Biosystems Engineering*, vol. 192, pp. 199–214, 2020.

[19] D. Briassoulis, G. Dougka, D. Dimakogianni, and I. Vayas, "Analysis of the collapse of a greenhouse with vaulted roof," *Biosystems Engineering*, vol. 151, pp. 495–509, 2016.

[20] J. Ren, J. Wang, S. Guo et al., "Finite element analysis of the static properties and stability of a large-span plastic greenhouse," *Computers and Electronics in Agriculture*, vol. 165, Article ID 7567591, 2019.

[21] R.-w. Kim, I.-b. Lee, U.-h. Yeo, and S.-y. Lee, "Evaluation of various national greenhouse design standards for wind loading," *Biosystems Engineering*, vol. 188, pp. 136–154, 2019.

[22] T. Ha, J. Kim, B.-H. Cho et al., "Finite element model updating of multi-span greenhouses based on ambient vibration measurements," *Biosystems Engineering*, vol. 161, pp. 145–156, 2017.

[23] D. J. Hur and S. Kwon, "Fatigue analysis of greenhouse structure under wind Load and self-weight," *Applied Sciences*, vol. 7, no. 12, pp. 1–11, 2017.

[24] D. J. Hur, J. H. Noh, and H. J. Lee, "Evaluation of stress distribution with wind speed in a greenhouse structure," *Wind and Structures*, vol. 27, no. 5, pp. 347–356, 2018.

[25] D. Ma, J. X. Zhang, H. Y. Duan et al., "Reutilization of gangue wastes in underground backfilling mining: overburden aquifer protection," *Chemosphere*, vol. 264, pp. 1–13, Article ID 128400, 2021.

[26] D. Ma, H. Duan, Q. Zhang et al., "A numerical gas fracturing model of coupled thermal, flowing and mechanical effects," *Computers, Materials & Continua*, vol. 65, no. 3, pp. 2123–2141, 2020.

[27] J. Y. Yan, L. Zhou, C. J. Zhou et al., "Method for calculating basic wind pressure of plastic greenhouse," *Transactions of the Chinese Society of Agricultural Engineering*, vol. 30, no. 12, pp. 171–176, 2014.

[28] L. L. Wang, *Foundation of Stress Waves*, pp. 274–276, National Defense Industry Press, Beijing, China, 2005.

[29] N. S. Abhyankar, "Flexural waves in beams with geometrical and material longitudinal discontinuities," *International Journal of Impact Engineering*, vol. 9, no. 2, pp. 205–222, 1990.

[30] B. C. Huang, *Principle and Application of Structural Wind Resistance Analysis*, pp. 46-47, Tongji University Press, Shanghai, China, 2001.

[31] J. Chen, Y. Chen, Y. Peng et al., "Stochastic harmonic function based wind field simulation and wind-induced reliability of super high-rise buildings," *Mechanical Systems and Signal Processing*, vol. 133, pp. 1–20, Article ID 106264, 2019.